Published in final edited form as:

Nat Med. 2016 June ; 22(6): 632–640. doi:10.1038/nm.4092.

An oncogenic *Ezh2* mutation cooperates with particular genetic alterations to induce tumors in mice and redistributes H3K27 trimethylation throughout the genome

George P. Souroullas[1,2], **William R. Jeck**[1,2], **Joel S. Parker**[2], **Jeremy M. Simon**[2], **Jie-Yu Liu**[1,2], **Joshiawa Paulk**[3], **Jessie Xiong**[2], **Kelly S. Clark**[2], **Yuri Fedoriw**[2,4], **Jun Qi**[3], **Christin E. Burd**[5], **James E. Bradner**[3,6], and **Norman E. Sharpless**[1,2,+]

[1]Department of Genetics, University of North Carolina School of Medicine, Chapel Hill, North Carolina, USA

[2]The Lineberger Comprehensive Cancer Center, University of North Carolina School of Medicine, Chapel Hill, North Carolina, USA

[3]Department of Medical Oncology, Dana-Farber Cancer Institute, Harvard Medical School, Boston, Massachusetts, USA

[4]Department of Pathology and Laboratory Medicine, University of North Carolina School of Medicine, Chapel Hill, North Carolina, USA

[5]The Ohio State University, Departments of Molecular Genetics and Molecular Virology, Immunology and Medical Genetics, Columbus, Ohio, USA

[6]Department of Medicine, Harvard Medical School, Boston, Massachusetts, USA

Abstract

B-cell lymphoma and melanoma harbor recurrent mutations in the gene encoding the EZH2 histone methyltransferase, but the carcinogenic role of these mutations is unclear. Here we describe a mouse model in which the most common somatic *EZH2* gain-of-function mutation (Y646F in human, Y641F in the mouse) can be conditionally expressed. Expression of $Ezh2^{Y641F}$ in mouse B-cells or melanocytes caused high-penetrance lymphoma or melanoma, respectively. Bcl2 overexpression or p53 loss, but not c-Myc overexpression, further accelerated lymphoma progression, and expression of mutant B-Raf but not mutant N-Ras further accelerated melanoma progression. Although expression of $Ezh2^{Y641F}$ increased abundance of global H3K27 trimethylation (H3K27me3), it also caused a widespread redistribution of this repressive mark,

+Address correspondence to: Norman E. Sharpless, The Lineberger Comprehensive Cancer Center, University of North Carolina School Medicine, CB #7295, Chapel Hill, North Carolina 27599, USA, Phone: (919) 966-1185, Fax: (919) 966-8212, NES@med.unc.edu.

Accession numbers: GSE79036

Author contributions

G.P.S and N.E.S conceived the study, designed experiments and wrote the manuscript. G.P.S, J.-Y.L, J.X, J.P and K.S.C performed experiments. G.P.S, W.R.J, J.S.P and J.M.S analyzed sequencing data. Y.F performed animal histopathology. C.E.B generated the N-Ras animal models. J.E.B, J.Q designed and synthesized JQEZ5. G.P.S, N.E.S, J.E.B, J.Q and C.E.B performed data interpretation.

including a loss of H3K27me3 associated with increased transcription at many loci. These results suggest that Ezh2^{Y641F} induces lymphoma and melanoma through a vast reorganization of chromatin structure inducing both repression and activation of polycomb-regulated loci.

INTRODUCTION

Data from several cancer types suggest that dysregulation of polycomb group complexes (PcGs) can contribute to malignant transformation, consistent with the fact that PcG complexes regulate thousands of transcripts responsible for cell fate[1–3]. The role of PcG-mediated gene silencing in cancer is supported by the observation that many cancers harbor higher levels or activating mutations of PcG genes. Moreover, PcG-repressed genes include tumor suppressors like the *INK4a/ARF* (*CDKN2a*) locus[4–6].

EZH2 (Enhancer of Zeste Homolog 2) is the catalytic component of the Polycomb repressive complex group 2 (PRC2) and was first identified in *Drosophila* for its role in development and differentiation. EZH2 is highly expressed in different types of B-cell tumors[7,8], and along with PcG proteins EED and BMI, is critical to B-cell development[9–11]. Sequencing studies identified frequent mutations in the EZH2 SET-domain (e.g. tyrosine residue 646 (Y646, equivalent to Y641 in the mouse)) in germinal center (GC) diffuse large B-cell lymphoma (DLBCL) and follicular lymphomas[12–14]. Somatic EZH2 mutations or amplifications also occur in other tumor types, including non-small cell lung cancer, prostate cancer, colon carcinoma and melanoma[15–17], whereas loss-of-function events appear in MDS/AML[18] and T-cell ALL[19]. These findings suggest that EZH2 may be a potential therapeutic target beyond lymphoma, with currently five open clinical trials using three different Ezh2 inhibitors (GSK, Epizyme and Constellation).

No mouse model of the most common EZH2 SET-domain mutations is currently available to investigate its cell-dependent *in vivo* effect or to test the efficacy of EZH2-targeted therapeutics. To understand the role and function of this mutation in malignant progression, we generated a model permitting conditional expression of the mutant protein ‘knocked-in’ to the native locus with intact cis-regulatory elements. We examined the ability of this allele to promote lymphoid and solid (*e.g.* melanoma) malignancies by itself, and in co-operation with other oncogenic events, by crossing to mouse strains expressing tissue-specific Cre-recombinase.

RESULTS

Expression of Ezh2^{Y641F} promotes lymphoma

We validated expression of the Ezh2^{Y641F} allele by Southern blot, PCR and qRT-PCR (Fig. 1a, Supplementary Fig. 1a–d). In the absence of CRE-mediated recombination, the allele produces a wild-type transcript (Fig. 1a) and upon CRE-mediated deletion of a floxed ‘mini-gene’, it expresses the Y641F mutant, which is equivalent to the most common *EZH2* missense mutation (Y646F) in human cancers [15,17]. To assess functionality *in vivo*, we crossed the *Ezh2*$^{Y641F/+}$ allele to *CD19*$^{CRE/+}$ mice, which constitutively express CRE recombinase in B-lymphocytes[20]. CD19 positive B-cells from 8-week-old *CD19*$^{CRE/+}$ and

CD19$^{CRE/+}$*Ezh2*$^{Y641F/+}$ mice expressed *Ezh2* transcripts at equal levels (Supplementary Fig. 1e). Consistent with a reported gain-of-function of the Y641F mutation in humans[21], B-cells from 8-week-old *CD19*$^{CRE/+}$*Ezh2*$^{Y641F/+}$ mice exhibited a ~3-fold increase in H3K27me3 compared to matched B-cells from *CD19*$^{CRE/+}$*Ezh2*$^{+/+}$ mice and CD19^{-} cells (Fig. 1b). Expression of Ezh2^{Y641F} had minimal effect on B-cell development in 8-week old mice (Supplementary Fig. 2a–h).

To examine the effects of *Ezh2*^{Y641F} on B-cell malignancy, we longitudinally observed a cohort of littermate *CD19*$^{CRE/+}$*Ezh2*$^{Y641F/+}$ and *CD19*$^{CRE/+}$*Ezh2*$^{+/+}$ animals. In contrast to results employing animals expressing Ezh2^{Y641F} under the control of a collagen promoter[22], expression of Ezh2^{Y641F} from the endogenous locus induced highly penetrant B-cell lymphoma with a median survival of one year (Fig. 1c). All tumors analyzed ($n = 15$) from *CD19*$^{CRE/+}$*Ezh2*$^{Y641F/+}$ mice demonstrated recombination of the *Ezh2* allele (not shown) and a CD45+ B220+ CD19+ IgM+ CD43+ CD5+ phenotype; they also expressed the myeloid marker Mac1 (Supplementary Fig. 3a). Tumor-bearing mice demonstrated disruption of the splenic architecture and expansion of abnormal, large lymphoid cells in the white pulp, with ~50% of animals demonstrating frank leukemia and/or hepatic involvement (Supplementary Fig. 3b). Tumors exhibited increased expression of H3K27me3 and were readily transplantable into syngeneic recipients (Fig. 1d, and Supplementary Fig. 3c–e). Therefore, physiological expression of Ezh2^{Y641F} in young mice does not markedly perturb the development of B-lymphocytes, but facilitates malignant transformation.

To determine whether genetic alterations detected in human B-cell lymphomas cooperate with *Ezh2*^{Y641F} in tumor formation, we transduced hematopoietic progenitors from *CD19*$^{CRE/+}$*Ezh2*$^{+/+}$ or *CD19*$^{CRE/+}$*Ezh2*$^{Y641F/+}$ mice with retroviruses encoding Bcl2 or c-Myc. Expression of c-Myc subtly increased B-cell lymphocytosis (Supplementary Fig. 4a), but did not accelerate tumor formation in *CD19*$^{CRE/+}$*Ezh2*$^{Y641F/+}$ mice (Fig. 1e). Consistent with a prior report[22], recipients of Bcl2-transduced *CD19*$^{CRE/+}$*Ezh2*$^{Y641F/+}$ hematopoietic progenitors developed advanced B-cell lymphoma much faster than recipients of Bcl2-transduced *CD19*$^{CRE/+}$*Ezh2*$^{+/+}$ cells (Fig. 1e, $P < 0.001$, Supplementary Fig. 4b, c). Moreover, the combination of somatic *p53* inactivation with Ezh2^{Y641F} expression accelerated lymphoma formation (Fig. 1f, $P < 0.001$, Supplementary Fig. 4d,e). These results suggest that globally increased H3K27me3 cooperates with apoptotic resistance mediated by Bcl2 overexpression or *p53* loss to accelerate B-cell transformation, consistent with the co-occurrence of these genetic alterations in human B-cell lymphoma[23].

In vitro, EZH2^{Y641F} exhibits decreased H3K27 mono-methylase activity, but increased di- and tri-methylase activity compared to EZH2$^{+/+}$ [21,24], suggesting that transformation may require expression of both wild-type and mutant proteins. Consistent with this model, to our knowledge, all human cancers observed to date harboring *EZH2*^{Y641F} mutations also retain a wild-type copy of *EZH2*[13,15,17,23]. To test the requirement of wild-type Ezh2 for tumorigenesis, we determined the tumor latency of *CD19*$^{CRE/+}$*Ezh2*$^{Y641F/Y641F}$ mice. *CD19*$^{CRE/+}$*Ezh2*$^{Y641F/Y641F}$ mice developed splenomegaly and lymphadenopathy with an infiltration of abnormal B220^{low}Mac1^{low} B-cells (Fig. 1g, h) with kinetics and tumor immunophenotype nearly identical to *CD19*$^{CRE/+}$*Ezh2*$^{Y641F/+}$ mice. Both heterozygous and homozygous mice for the Y641F mutation exhibited elevated levels of H3K27me3

compared to controls (Fig. 1i). As both alleles from tumors of *Ezh2*$^{Y641F/Y641F}$ underwent recombination (Supplementary Fig. 4f) and therefore only express mutant Ezh2, these data demonstrate that wild-type Ezh2 function is dispensable for tumorigenesis in cells harboring Ezh2^{Y641F} mutations. This observation could reflect residual monomethylase activity of the tyrosine to phenylalanine substitution, which may not be a feature of other Y646 mutations of EZH2 [21]; it is also possible that another H3K27 monomethylase (e.g. EZH1) compensates for loss of EZH2 activity in these tumors.

Ezh2^{Y641F} cooperates with B-Raf but not N-Ras to induce melanoma

In addition to lymphoma, *EZH2*^{Y646} mutations are observed in 3% of human melanoma [25–27], with focal amplifications of *EZH2* noted in 15 of 262 (5.7%) of cases from the Cancer Genome Atlas (TCGA). As *B-RAF*^{V600E} or *N-RAS*^{Q61R} mutations occur in the majority of human melanomas, we tested the ability of the *Ezh2*^{Y641F} allele to cooperate with the conditionally activatable mouse alleles of *B-Raf*^{V600E} (ref. [28]) or *N-Ras*^{Q61R} (ref. [29]) in the presence of the tamoxifen-inducible tyrosinase CRE allele (*TyrCRE*^{ERT2}) [30,31]. Melanoma was not observed in *TyrCRE*^{ERT2}*B-Raf*^{V600} as previously described[29,32]. The inclusion, however, of a heterozygous *Ezh2*^{Y641F} mutation rapidly accelerated tumorigenesis of un-pigmented, non-metastatic melanoma in the context of *B-Raf*^{V600E} activation and combined *B-Raf*^{V600E}*Pten*$^{L/+}$ (Fig. 2a–c). *Ezh2*^{Y641F}, therefore, cooperates with mutant B-RAF (± haploinsufficiency of PTEN) in melanoma formation and maintenance.

In contrast, melanocyte-specific activation of *Ezh2*^{Y641F} in the presence of *N-Ras*^{Q61R} did not accelerate melanomagenesis, with or without *p16*^{Ink4a} loss (Fig. 2d). As *B-RAF* is thought to be a downstream effector of N-RAS signaling to MEK/ERK, the differing abilities of *N-Ras*^{Q61R} and *B-Raf*^{V600E} to promote melanoma in the context of *Ezh2*^{Y641F} was unexpected. We carefully examined data from prior melanoma sequencing studies[25–27] using cBIOPORTAL[15,17]. In accord with our murine genetic results, *EZH2* mutations in human melanoma co-occur at a significant frequency with activating mutations in *B-RAF (P = 0.006)*, and are mutually exclusive with *N-RAS* mutations *(P = 0.004)* (Supplementary Fig. 5). These results suggest that while RAF/MEK/ERK activation synergizes with *EZH2*^{Y641F} mutations in melanoma formation, a RAF-independent aspect of mutant RAS signaling renders the oncogenic effects of mutant EZH2 irrelevant to transformation.

We performed experiments to address the cooperation of EZH2 mutation with B-RAF but not N-RAS. We observed that the expression of N-RAS and B-RAF is not altered by the presence of the Y641F mutation (data not shown). A major pathway activated by N-RAS but not B-RAF is PI3K-AKT. To determine if mutant N-RAS but not B-RAF inhibits the oncogenic effects of Ezh2^{Y641F}, we transduced primary human melanocytes with B-RAF^{V600E}, N-RAS^{Q61K} or PIK3CA-CAAX, a membrane-bound and constitutively active catalytic subunit of PI3K. As previously reported[33], expression of each resulted in oncogene-induced senescent, as characterized by increased expression of *p16*^{INK4a} (Fig. 2e), ceased proliferation and flat enlarged morphology (data not shown). Neither B-RAF^{V600E}, N-RAS^{Q61K} nor PIK3CA-CAAX significantly altered EZH2 mRNA levels (Fig. 2f), however, N-RAS^{Q61K} and PIK3CA-CAAX, but not B-RAF^{V600E}, resulted in a global

decrease in H3K27me3 levels (Fig. 2g). This result is consistent with prior reports suggesting that activated AKT induces genome-wide changes in H3K27me3 (ref. [34]) via phosphorylation and suppression of EZH2[35]. These experiments suggest RAS-PI3K activation attenuates the oncogenic effects of $Ezh2^{Y641F}$, explaining the inability of $N\text{-}Ras^{Q61K}$ to accelerate melanoma formation.

Ezh2 activity is required for tumor maintenance

Next we investigated whether Ezh2 inhibition could suppress tumor growth in these mice. shRNA-mediated knock-down of Ezh2 in cell lines derived from the mouse melanomas described above resulted in significant growth inhibition *(P < 0.01,* Fig. 3a,b), suggesting that Ezh2 is required not only for tumor initiation but also maintenance. To determine the importance of Ezh2 enzymatic activity, we supplemented these genetic results with a pharmacological approach. We treated cell lines derived from $TyrCRE^{ERT2}B\text{-}Raf^{V600}Ezh2^{Y641F/+}$ melanoma with three EZH2 inhibitors: UNC1999 (ref. [36]), GSK126 (ref. [37]) and a previously unpublished SAM-competitive pyridinone inhibitor, JQEZ5. The Constellation and Epizyme inhibitors were not available to us for comparative analysis at the times of these studies. JQEZ5 was designed as an open-source compound with high potency and bioavailability, is ~10-fold selective for EZH2 over EZH1, and exhibits *in vitro* activity against the Y646F mutant in a homogenous assay (Supplementary Fig. 6a, b). In a panel of $Ezh2^{+/+}$ or $Ezh2^{Y641F}$ melanoma cell lines, UNC1999 and GSK126 showed EC50s of greater than 3.5μM regardless of *Ezh2* genotype (ratio of average $EC50^{WT}/EC50^{Y641F} = 1.4$ for both agents, Supplementary Fig. 6c). In contrast, JQEZ5 was nearly 5-fold more potent in $Ezh2^{Y641F}$ melanoma cell lines than in wild-type cell lines ($EC50^{Y641F}$ = 860nM vs. $EC50^{WT}$ = 4.0μM, Supplementary Fig. 6c, d). Treatment with all three compounds resulted in decreased H3K27me3 levels, with JQEZ5 being effective at nanomolar concentrations (Fig. 3c, d, Supplementary Fig. 7a, b). All three compounds induced cell cycle arrest within 3–5 days of treatment at their respective EC50s (Fig. 3e). Sub-micromolar exposures of JQEZ5 of greater than 1 week also induced cell death in $Ezh2^{Y641F}$ mutant lines (Supplementary Fig. 7c, d). To determine if Ezh1, an Ezh2 homolog, was responsible for residual H3K27me3 signal after Ezh2 inhibition (Fig. 3c, d), we knocked down Ezh1 in mutant melanoma cell lines treated with JQEZ5. Ezh1 knockdown did not affect cell growth or global H3K27me3 levels in inhibitor-treated $Ezh2^{+/+}$ or $Ezh2^{Y641F}$ cell lines (Supplementary Fig. 8), suggesting that Ezh1 does not compensate for Ezh2 inhibition in these melanomas.

We next assessed the anti-tumor efficacy of EZH2 inhibitors *in vivo*. We studied lymphoma in $CD19^{CRE}Ezh2^{Y641F+}$ mice with autochthonous tumors, and melanoma in immunodeficient mice transplanted with cell lines derived from the tumors of $TyrCRE^{ERT2}B\text{-}Raf^{V600E}Pten^{L/+}Ezh2^{Y641F/+}$ or $TyrCRE^{ERT2}B\text{-}Raf^{V600E}Pten^{L/L}$ mice. Once tumors reached 10 mm^3 in size, mice were treated with vehicle, the B-Raf inhibitor Dabrafenib (25mpk daily), JQEZ5 (50mpk, daily), or a combination of both. JQEZ5 was selected for these studies as it was the most efficacious compound *in vitro*, exhibited low toxicity, with favorable pharmacokinetic properties *in vivo,* comparable to those of Ezh2 inhibitors currently in clinical trials (Supplementary Fig. 6c–e). As single agents, Dabrafenib and JQEZ5 resulted in tumor growth inhibition in both $Ezh2^{+/+}$ and $Ezh2^{Y641F/+}$ tumors,

with Dabrafenib being the more potent agent. Combinatorial treatment with Dabrafenib and JQEZ5 resulted in additive activity in *Ezh2*$^{Y641F/+}$ but not *Ezh2*$^{+/+}$ tumors (Fig. 3f). After developing lymphoma as assessed by the appearance of pathological symptoms, *CD19*$^{CRE/+}$*Ezh2*$^{Y641F/+}$ animals were treated with vehicle or 50mpk of JQEZ5 by daily intraperitoneal injection. Six days of treatment with JQEZ5 complete cleared the malignant population (B220^{low}Mac1^{low}) from the spleen, without depleting normal B-cells (Fig. 3g, h, Supplementary Fig. 6f). These data show that a selective inhibitor of EZH2 has potent single-agent activity *in vivo* in an autochthonous model of *Ezh2*^{Y641F}-mutant B-cell lymphoma, and is effective in combination with a B-RAF inhibitor in RAF-mutant melanoma.

Effects of Ezh2^{Y641F} on RNA expression

To understand the molecular effects of Ezh2 activation in B-cells and melanoma, we performed RNA-seq and H3K27me3 chromatin immunoprecipitation and sequencing (ChIP-seq). As the expression of Ezh2^{Y641F} in young adult mice did not alter B-cell development (Supplementary Fig. 2), for B-cell analysis, we examined CD19+ cells isolated from the spleen of 8-week-old *CD19*$^{CRE/+}$*Ezh2*$^{Y641F/+}$ and *CD19*$^{CRE/+}$*Ezh2*$^{+/+}$ littermates. For melanoma experiments, we screened >20 cell lines derived from tumors of *TyrCRE*^{ERT2}*B-Raf*^{V600}*Pten*$^{L/+}$*Ezh2*$^{Y641F/+}$ mice, and sub-cloned two lines that had not recombined the *Ezh2* allele. Through *in vitro* 4-OH-tamoxifen treatment, these lines yielded isogenic lines differing only in expression of the *Ezh2* mutation. In B-cells, 213 transcripts were upregulated and 346 were repressed by *Ezh2*^{Y641F} ($P < 0.01$, Supplementary Table 1), whereas 563 genes were upregulated and 746 were downregulated in the *Ezh2*^{Y641F} melanoma cells ($P < 0.01$, Supplementary Table 2). Gene set enrichment analysis (GSEA) in both B-cells and melanoma cell lines expressing *Ezh2*^{Y641F} revealed a significant concordance between genes downregulated in cells expressing EZH2^{Y641F} and genes silenced by the PRC2 complex [38,39] (Fig. 4a, Supplementary Table 3). In separate biological replicates, we confirmed by qRT-PCR the altered expression of 8 transcripts identified by RNA-seq (Supplementary Fig. 9).

The RNA-seq analysis yielded two surprising results. First, in B-cells, GSEA indicated that transcripts repressed by expression of Ezh2^{Y641F} were enriched for genes known to be repressed by C-MYC activation in other B-lineage cells[40–42] (Fig. 4b; Supplementary Fig. 10a, b; Supplementary Table 3). Enrichment for C-MYC targets was also observed in Ezh2^{Y641F} expressing melanoma cell lines, albeit with less significance than in lymphoma (Supplementary Table 3). To directly assess the relationship between C-MYC and EZH2 in B-cells, we first used a B-cell lymphoma line (P493-6)[43] with tet-inducible C-MYC expression. Upon activation of C-MYC, EZH2 expression increased in a time-dependent manner (Fig. 4c), resulting in increased global H3K27me3 (Fig. 4d). We next analyzed C-MYC ChIP datasets available through the ENCODE consortium, looking for enrichment of C-MYC and MAX (a dimerization partner of C-MYC) at the *EZH2* locus. Our analysis showed multiple C-MYC/MAX binding sites at the *EZH2* transcription start site (TSS), in the *EZH2* promoter, and at an enhancer ~50 kb 5′ to the TSS in multiple cell types, including lymphoma (Supplementary Fig 10c). The C-MYC/MAX binding peaks were associated with strong peaks of H3K27 acetylation (H3K27Ac, Supplementary Fig. 10c),

suggesting transcriptional activation. These findings agree with prior studies of C-MYC and EZH2 expression[44,45], and suggest that some of the oncogenic effects of C-MYC amplification in B-cell lymphoma may be mediated by EZH2 activation.

A second surprising finding of the RNA-seq analysis of *Ezh2*^{Y641F} cells was an increase in the expression of many genes known to be directly repressed by the PRC2 complex and EZH2, such as *Hoxc4*, *Hoxc9* and *Meis1* in B-cells (Supplementary Fig. 9, Supplementary Table 1) and the *Hoxd* gene cluster in melanoma cell lines (Supplementary Table 2). Mining Epigenomics Roadmap[46] data, we noted that many of the PRC2-regulated genes activated by Ezh2^{Y641F} were densely covered with repressive H3K27me3 in normal B-cells, suggesting they are silenced in healthy cells (Supplementary Fig. 11a). In contrast, many of the genes most strongly repressed by Ezh2^{Y641F} lacked H3K27me3 in normal B-cells, and instead were located near enhancer elements marked with H3K27Ac (Supplementary Fig. 11b). This suggests that Ezh2^{Y641F} activates certain silenced genes and silences certain activated genes.

Ezh2^{Y641F} expression causes global re-distribution of H3K27me3

To determine if this apparent pattern was a direct effect of altered H3K27me3 abundance, we performed H3K27me3 ChIP-seq. Principal component analysis (PCA, Fig. 5a) of the differentially expressed ChIP-seq peaks showed that the first PC of the dataset reflected Ezh2 genotype, whereas a second, weaker PC reflected tissue of origin (B-cells vs. melanoma). Treatment with JQEZ5 altered the peak pattern in Ezh2-mutant melanoma cell lines along the first PC towards untreated isogenic WT cells (Fig. 5a), suggesting EZH2 inhibition significantly 'normalized' the peak pattern in Ezh2^{Y641F} expressing cells. This impression was confirmed when H3K27me3 was visualized across the entire genome (Supplementary Fig. 12a).

We next performed hierarchical clustering of these samples by genome-wide, non-overlapping 5 kb windows that exhibited dynamic H3K27me3 between *Ezh2*$^{+/+}$ and matched *Ezh2*$^{Y641F/+}$ cells based on a standard deviation threshold (Supplementary Fig. 12b, c). This analysis revealed two major clusters: one with increased H3K27me3 in *Ezh2*$^{+/+}$ samples, and a larger cluster with increased H3K27me3 in *Ezh2*$^{Y641F/+}$ samples. These clusters appeared in both B-cells and melanoma cells with significant overlap of dynamic regions (Supplementary Fig. 12b, c). The finding of a large number of loci with dense H3K27me3 in *Ezh2*$^{+/+}$ samples that is lost in *Ezh2*$^{Y641F/+}$ B-cells or melanoma was unexpected given the presumed hypermorphic activity of the mutant enzyme, yet such loci were even more obvious using a 'peak calling' algorithm (MACS[47]), which assigns statistical significance to each dynamic peak. A 'volcano plot' of the log-transformed fold-change of H3K27me3 peak signal versus log transformed *P* value demonstrated that the peaks with most highly significant change between *Ezh2*$^{+/+}$ and *Ezh2*$^{Y641F/+}$ samples were those that decreased 2–4 fold in *Ezh2*$^{Y641F/+}$ cells. As in the PCA, there was a significant restoration of the wild-type peak pattern in *Ezh2*$^{Y641F/+}$ melanoma cells by JQEZ5 treatment (Fig. 5b, Supplementary Fig. 12a). We considered the possibility that this apparent decrease in peaks in *Ezh2*$^{Y641F/+}$ cells reflected an artifact of normalization, as a relative increase in genome-wide H3K27me3 could dilute the intensity of the highest peaks seen in *Ezh2*$^{+/+}$ cells. However, we discounted this possibility for two reasons. First, the fold-decrease of

H3K27me3 at certain loci (Fig. 5b) greatly exceeded the global increase in H3K27me3 by western analysis (Fig. 1b, j), suggesting dilution alone as an unlikely cause. Moreover, the observed changes in peak height correlated with RNA expression at specific loci: for example, the significant increase in *HoxC* expression in *Ezh2*$^{Y641F/+}$ B-cells correlated with H3K27me3 loss at this locus (Fig. 5c), whereas *Igf1* repression in *Ezh2*$^{Y641F/+}$ melanoma cells lines occurred in the setting of greatly increased H3K27me3 at this locus (Fig. 5c). These observations suggest that the expression of mutant Ezh2 causes a global re-distribution of H3K27me3, from highly focal peaks apparent in *Ezh2*$^{+/+}$ samples to a larger number of broader, less focal peaks in *Ezh2*$^{Y641F/+}$ samples, with attendant changes in gene expression.

We analyzed the effects of Ezh2^{Y641F} expression on the distribution of H3K27me3 at promoter regions, TSS and gene bodies. Toward that end, we rank-ordered transcripts by level of expression in *Ezh2*$^{+/+}$ samples, and averaged the normalized H3K27me3 intensity ± 5 kb around the TSS for the top and bottom quartiles of expression (Fig. 5d). Consistent with prior work [48], this analysis showed increased H3K27me3 flanking the TSS of genes with the lowest expression (black), with an obvious 'spike' of H3K27me3 immediately 3′ to the TSS. Expression of Ezh2^{Y641F} led to a relative decrease in H3K27me3 in the least transcribed genes with little effect on H3K27me3 at transcripts in the highest quartile of expression. This observation suggests that the increased expression of some transcripts in Ezh2^{Y641F} mutant cells (Supplementary Table 1, 2) results from a paradoxical loss of H3K27me3 around the TSS's of certain PRC2-repressed genes.

We next analyzed mean normalized H3K27me3 signal around the TSS (± 5 kb) of genes with a significant change in expression between *Ezh2*$^{+/+}$ and *Ezh2*$^{Y641F/+}$ cells (Supplementary Table 1 and 2). Genes upregulated in the presence of Ezh2^{Y641F} in both B-cells and melanoma cell lines exhibited decreased H3K27me3 signal around the TSS, particularly immediately 3′ to the TSS (Fig. 5e-left). In contrast, genes that were downregulated in the presence of Ezh2^{Y641F} exhibited increased H3K27me3, starting on average more than 2 kb downstream of TSS (Fig. 5e-right). These results are consistent with a prior report suggesting H3K27me3 in the gene body is strongly repressive, whereas promoter H3K27me3 can also be seen in actively transcribed genes[48]. To further consider this possibility, we analyzed H3K27me3 along the gene body [from TSS to Transcription Termination Site (TTS)] of transcripts differentially expressed between *Ezh2*$^{+/+}$ and *Ezh2*$^{Y641F/+}$ samples (Fig. 5f). In contrast to the effects of *Ezh2* mutations around the TSS, we observed a modest effect of *Ezh2*^{Y641F} on upregulated genes ($P = 0.07$), but a marked increase ($P = 1.7e\text{-}15$) of H3K27me3 in the gene body of downregulated genes (Fig. 5f).

Finally, we analyzed the effect of the *Ezh2*^{Y641F} mutation on the entire genome, focusing on melanoma cell lines. Toward this end, we identified broad H3K27me3 domains in *Ezh2*$^{+/+}$ cells across the genome, and then compared the mean, normalized H3K27me3 signal 10 kb upstream and downstream of these domains in *Ezh2*$^{+/+}$ vs. *Ezh2*$^{Y641F/+}$ samples. Consistent with our peak-calling analysis (Fig. 5b), we observed a dramatic decrease in H3K27me3 in *Ezh2*$^{Y641F/+}$ samples, which was largely restored with JQEZ5 treatment. Importantly, however, we observed an increase in H3K27me3 extending for more than 10 kb both 5′ and 3′ to these domains in *Ezh2*$^{Y641F/+}$ samples (Fig. 5g). In aggregate, these results demonstrate

that the *Ezh2*^{Y641F} mutant enzyme causes a global redistribution of H3K27me3 away from focal peaks (e.g. near the TSS) across broad regions including gene bodies and intergenic regions.

DISCUSSION

Consistent with prior work [21], we show that under physiological conditions, global H3K27me3 levels are elevated in cells expressing Ezh2^{Y641F}, consistent with a model of increased enzymatic activity. On the other hand, through H3K27me3 ChIP-seq analysis, we provide evidence that the Y641F mutation does not monotonically increase H3K27me3, but rather redistributes the H3K27me3 mark across the genome with complex effects on transcription. Through integrated analysis of ChIP-seq and RNA-seq, we observe loci where Ezh2^{Y641F} samples show reduced H3K27me3 and increased expression, and vice versa. In particular, we note that the effects are not uniform with regard to genomic regions: the mutation seems to favor H3K27me3 over large regions—at gene bodies and intergenic regions—at the expense of focal peaks near the TSS. While the mechanistic basis for this preference in unclear, the recent solution of the crystal structure of the yeast (*C. Thermophilus*) PRC2 complex provides tantalizing clues[49]. In this work, the authors suggest that wild-type EZH2 is allosterically activated when EED binds H3K27me3, through reorganization of the complex that alters the lysine substrate channel of the enzyme in a manner similar to the A682 SET domain mutation[50]. This structure suggests that the yeast amino acid (Y826) homologous to Y646 also participates in the formation of this substrate channel, providing the possibility that this mutation reduces the need for H3K27me3-EED stimulation of the enzymatic complex, thereby creating a more promiscuous complex. Such a complex would be expected to increase H3K27me3 at most nucleosomes. If some co-factor (e.g. SAM) for tri-methylation were limiting, however, such a complex might also show reduced H3K27me3 at focal peaks that perhaps more strongly require the stimulatory effects of the H3K27me3-EED interaction in cells expressing the wild-type complex. Regardless of the precise mechanistic details, however, the observations that Ezh2^{Y641F} expression decreases H3K27me3 at many loci (Fig. 5b–g; Supplementary Fig. 12) and that this effect is largely reversed with an EZH2 *inhibitor* (Fig. 5b, g; Supplementary Fig. 12a) are not consistent with the notion that this is a strictly hypermorphic allele. Rather, we believe the allele should more properly be considered neomorphic, perhaps as a result of reduced requirements for H3K27me3-mediated auto-activation.

Therapeutically, these results have direct implications for human cancers harboring SET domain mutations of *Ezh2*. First, the overlap of gene-expression signatures of Ezh2 activation and c-Myc repression in B-lineage cancers (Fig. 4b) and lack of cooperation between c-Myc over-expression and Ezh2 mutation in lymphomagenesis (Fig. 1e) suggests the intriguing possibility that EZH2 mediates some of the transforming effects of C-MYC in lymphoma. Just as recent reports suggesting *BAP1*[51], *ARID1a* [52] and *SNF5* [53] mutations predict sensitivity to EZH2 inhibitors, this finding suggests a rationale for testing EZH2 inhibitors in B-cell neoplasms characterized by strong C-MYC activation. Additionally, we report a newly developed, potent pharmacologic EZH2 inhibitor, JQEZ5, with excellent *in vitro* and *in vivo* properties and which demonstrates marked *in vivo* anti-tumor activity in a faithful model of Ezh2 mutant cancer (Fig. 3, Supplementary Fig. 6). Lastly, the discovery of

the exquisite and specific cooperation between activating genetic events of EZH2 and B-RAF, but not N-RAS (Fig. 2, Supplementary Fig. 5), predicts synergistic activity of combined therapy with RAF inhibitors (e.g. dabrafenib or vemurafenib) and EZH2 inhibitors in this heretofore unappreciated melanoma sub-type representing 3–9% of all melanoma patients.

Supplementary Material

Refer to Web version on PubMed Central for supplementary material.

Acknowledgments

We thank the UNC Lineberger Animal Histopathology Core, Flow Cytometry Core, Animal Models Core and Microscopy Services Laboratory for technical assistance; the Mouse Phase I Unit (D. Darr and J. Roques) for providing animals and expertise. This work was supported by grants from the NCI (N.E.S, R01-CA163896), NIA (N.E.S, R01-AG024379), NHLBI (G.P.S, F32-HL117581) and NCI (G.P.S, T32-CA009156).

References

1. Bernstein BE, et al. A bivalent chromatin structure marks key developmental genes in embryonic stem cells. Cell. 2006; 125:315–326. [PubMed: 16630819]
2. Boyer LA, et al. Polycomb complexes repress developmental regulators in murine embryonic stem cells. Nature. 2006; 441:349–353. [PubMed: 16625203]
3. Bracken AP, Dietrich N, Pasini D, Hansen KH, Helin K. Genome-wide mapping of Polycomb target genes unravels their roles in cell fate transitions. Genes & development. 2006; 20:1123–1136. [PubMed: 16618801]
4. Bracken AP, et al. The Polycomb group proteins bind throughout the INK4A-ARF locus and are disassociated in senescent cells. Genes & development. 2007; 21:525–530. [PubMed: 17344414]
5. Kotake Y, et al. pRB family proteins are required for H3K27 trimethylation and Polycomb repression complexes binding to and silencing p16INK4alpha tumor suppressor gene. Genes & development. 2007; 21:49–54. [PubMed: 17210787]
6. Chen H, et al. Polycomb protein Ezh2 regulates pancreatic beta-cell Ink4a/Arf expression and regeneration in diabetes mellitus. Genes & development. 2009; 23:975–985. [PubMed: 19390090]
7. Raaphorst FM, et al. Coexpression of BMI-1 and EZH2 polycomb group genes in Reed-Sternberg cells of Hodgkin's disease. The American journal of pathology. 2000; 157:709–715. [PubMed: 10980109]
8. Visser HP, et al. The Polycomb group protein EZH2 is upregulated in proliferating, cultured human mantle cell lymphoma. British journal of haematology. 2001; 112:950–958. [PubMed: 11298590]
9. Su IH, et al. Ezh2 controls B cell development through histone H3 methylation and Igh rearrangement. Nature immunology. 2003; 4:124–131. [PubMed: 12496962]
10. Lessard J, et al. Functional antagonism of the Polycomb-Group genes eed and Bmi1 in hemopoietic cell proliferation. Genes & development. 1999; 13:2691–2703. [PubMed: 10541555]
11. van der Lugt NM, et al. Posterior transformation, neurological abnormalities, and severe hematopoietic defects in mice with a targeted deletion of the bmi-1 proto-oncogene. Genes & development. 1994; 8:757–769. [PubMed: 7926765]
12. Lohr JG, et al. Discovery and prioritization of somatic mutations in diffuse large B-cell lymphoma (DLBCL) by whole-exome sequencing. Proceedings of the National Academy of Sciences of the United States of America. 2012; 109:3879–3884. [PubMed: 22343534]
13. Morin RD, et al. Somatic mutations altering EZH2 (Tyr641) in follicular and diffuse large B-cell lymphomas of germinal-center origin. Nature genetics. 2010; 42:181–185. [PubMed: 20081860]
14. Pasqualucci L, et al. Inactivating mutations of acetyltransferase genes in B-cell lymphoma. Nature. 2011; 471:189–195. [PubMed: 21390126]

15. Cerami E, et al. The cBio cancer genomics portal: an open platform for exploring multidimensional cancer genomics data. Cancer discovery. 2012; 2:401–404. [PubMed: 22588877]
16. Forbes S, et al. Cosmic 2005. British journal of cancer. 2006; 94:318–322. [PubMed: 16421597]
17. Gao J, et al. Integrative analysis of complex cancer genomics and clinical profiles using the cBioPortal. Science signaling. 2013; 6:pl1. [PubMed: 23550210]
18. Nikoloski G, et al. Somatic mutations of the histone methyltransferase gene EZH2 in myelodysplastic syndromes. Nature genetics. 2010; 42:665–667. [PubMed: 20601954]
19. Ntziachristos P, et al. Genetic inactivation of the polycomb repressive complex 2 in T cell acute lymphoblastic leukemia. 2012; 18:298–303.
20. Rickert RC, Roes J, Rajewsky K. B lymphocyte-specific, Cre-mediated mutagenesis in mice. Nucleic acids research. 1997; 25:1317–1318. [PubMed: 9092650]
21. Sneeringer CJ, et al. Coordinated activities of wild-type plus mutant EZH2 drive tumor-associated hypertrimethylation of lysine 27 on histone H3 (H3K27) in human B-cell lymphomas. Proceedings of the National Academy of Sciences of the United States of America. 2010; 107:20980–20985. [PubMed: 21078963]
22. Beguelin W, et al. EZH2 is required for germinal center formation and somatic EZH2 mutations promote lymphoid transformation. Cancer cell. 2013; 23:677–692. [PubMed: 23680150]
23. Morin RD, et al. Frequent mutation of histone-modifying genes in non-Hodgkin lymphoma. Nature. 2011; 476:298–303. [PubMed: 21796119]
24. Yap DB, et al. Somatic mutations at EZH2 Y641 act dominantly through a mechanism of selectively altered PRC2 catalytic activity, to increase H3K27 trimethylation. Blood. 2011; 117:2451–2459. [PubMed: 21190999]
25. Hodis E, et al. A landscape of driver mutations in melanoma. Cell. 2012; 150:251–263. [PubMed: 22817889]
26. Alexandrov LB, et al. Signatures of mutational processes in human cancer. Nature. 2013; 500:415–421. [PubMed: 23945592]
27. Krauthammer M, et al. Exome sequencing identifies recurrent somatic RAC1 mutations in melanoma. Nature genetics. 2012; 44:1006–1014. [PubMed: 22842228]
28. Dankort D, et al. A new mouse model to explore the initiation, progression, and therapy of BRAFV600E-induced lung tumors. Genes & development. 2007; 21:379–384. [PubMed: 17299132]
29. Burd CE, et al. Mutation-specific RAS oncogenicity explains NRAS codon 61 selection in melanoma. Cancer discovery. 2014; 4:1418–1429. [PubMed: 25252692]
30. Bosenberg M, et al. Characterization of melanocyte-specific inducible Cre recombinase transgenic mice. Genesis. 2006; 44:262–267. [PubMed: 16676322]
31. Monahan KB, et al. Somatic p16(INK4a) loss accelerates melanomagenesis. Oncogene. 2010; 29:5809–5817. [PubMed: 20697345]
32. Dankort D, et al. Braf(V600E) cooperates with Pten loss to induce metastatic melanoma. Nature genetics. 2009; 41:544–552. [PubMed: 19282848]
33. Serrano M, Lin AW, McCurrach ME, Beach D, Lowe SW. Oncogenic ras provokes premature cell senescence associated with accumulation of p53 and p16INK4a. Cell. 1997; 88:593–602. [PubMed: 9054499]
34. Michaloglou C, et al. BRAFE600-associated senescence-like cell cycle arrest of human naevi. Nature. 2005; 436:720–724. [PubMed: 16079850]
35. Zuo T, et al. Epigenetic silencing mediated through activated PI3K/AKT signaling in breast cancer. Cancer research. 2011; 71:1752–1762. [PubMed: 21216892]
36. Konze KD, et al. An orally bioavailable chemical probe of the Lysine Methyltransferases EZH2 and EZH1. ACS Chem Biol. 2013; 8:1324–1334. [PubMed: 23614352]
37. McCabe MT, et al. EZH2 inhibition as a therapeutic strategy for lymphoma with EZH2-activating mutations. Nature. 2012; 492:108–112. [PubMed: 23051747]
38. Kamminga LM, et al. The Polycomb group gene Ezh2 prevents hematopoietic stem cell exhaustion. Blood. 2006; 107:2170–2179. [PubMed: 16293602]

39. Kondo Y, et al. Gene silencing in cancer by histone H3 lysine 27 trimethylation independent of promoter DNA methylation. Nature genetics. 2008; 40:741–750. [PubMed: 18488029]
40. Boylan KL, et al. A transgenic mouse model of plasma cell malignancy shows phenotypic, cytogenetic, and gene expression heterogeneity similar to human multiple myeloma. Cancer research. 2007; 67:4069–4078. [PubMed: 17483317]
41. Pasqualucci L, et al. AID is required for germinal center-derived lymphomagenesis. Nature genetics. 2008; 40:108–112. [PubMed: 18066064]
42. Mori S, et al. Utilization of pathway signatures to reveal distinct types of B lymphoma in the Emicro-myc model and human diffuse large B-cell lymphoma. Cancer research. 2008; 68:8525–8534. [PubMed: 18922927]
43. Pajic A, et al. Cell cycle activation by c-myc in a burkitt lymphoma model cell line. International journal of cancer. Journal international du cancer. 2000; 87:787–793. [PubMed: 10956386]
44. Sander S, et al. MYC stimulates EZH2 expression by repression of its negative regulator miR-26a. Blood. 2008; 112:4202–4212. [PubMed: 18713946]
45. Zhang X, et al. Coordinated silencing of MYC-mediated miR-29 by HDAC3 and EZH2 as a therapeutic target of histone modification in aggressive B-Cell lymphomas. Cancer cell. 2012; 22:506–523. [PubMed: 23079660]
46. Roadmap Epigenomics C et al. Integrative analysis of 111 reference human epigenomes. Nature. 2015; 518:317–330. [PubMed: 25693563]
47. Zhang Y, et al. Model-based analysis of ChIP-Seq (MACS). Genome biology. 2008; 9:R137. [PubMed: 18798982]
48. Young MD, et al. ChIP-seq analysis reveals distinct H3K27me3 profiles that correlate with transcriptional activity. Nucleic acids research. 2011; 39:7415–7427. [PubMed: 21652639]
49. Jiao L, Liu X. Structural basis of histone H3K27 trimethylation by an active polycomb repressive complex 2. Science. 2015; 350:aac4383. [PubMed: 26472914]
50. McCabe MT, et al. Mutation of A677 in histone methyltransferase EZH2 in human B-cell lymphoma promotes hypertrimethylation of histone H3 on lysine 27 (H3K27). 2012; 109:2989–2994.
51. LaFave LM, et al. Loss of BAP1 function leads to EZH2-dependent transformation. Nature medicine. 2015; 21:1344–1349.
52. Bitler BG, et al. Synthetic lethality by targeting EZH2 methyltransferase activity in ARID1A-mutated cancers. Nature medicine. 2015; 21:231–238.
53. Knutson SK, et al. Durable tumor regression in genetically altered malignant rhabdoid tumors by inhibition of methyltransferase EZH2. Proceedings of the National Academy of Sciences of the United States of America. 2013; 110:7922–7927. [PubMed: 23620515]

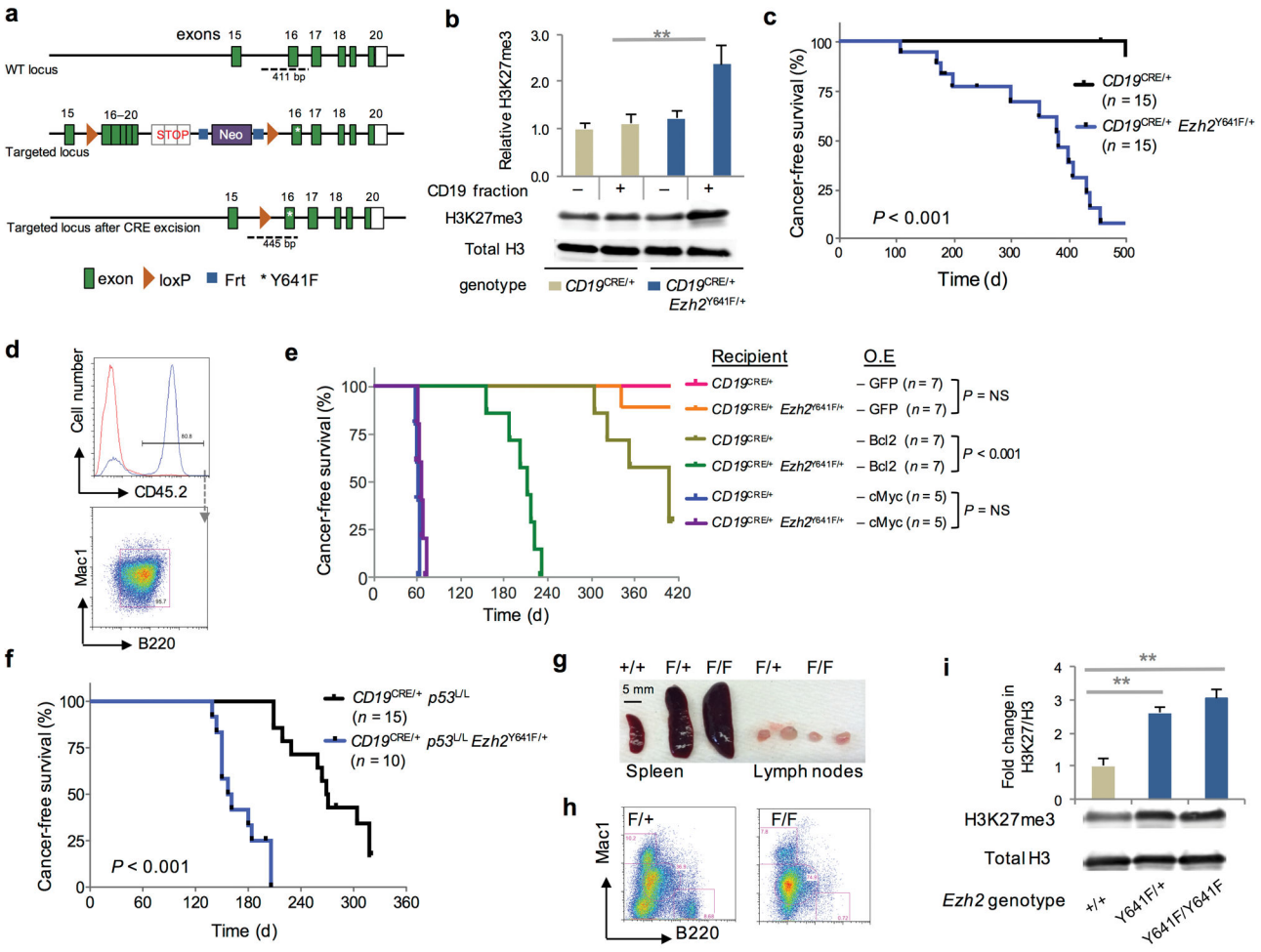

Figure 1. Design, oncogenic activity and genetic interactions of the *Ezh2*^{Y641F} allele in B-cells

a. Schematic of *Ezh2*^{Y641F} targeting strategy. * denotes Y641F mutation in exon 16.

b. Western blot analysis and quantification of total H3 and H3K27me3 in *CD19*$^{CRE/+}$*Ezh2*$^{+/+}$ vs *CD19*$^{CRE/+}$*Ezh2*$^{Y641F/+}$ mice. Error bars show standard error of the mean (SEM) for four independent experiments.

c. Kaplan-Meier analysis of lymphoma-free survival of littermate *CD19*$^{CRE/+}$ vs *CD19*$^{CRE/+}$*Ezh2*$^{Y641F/+}$ mice. Median cancer-free survival of *CD19*$^{CRE/+}$*Ezh2*$^{Y641F/+}$ mice is 383 days ($P < 0.001$, calculated using a log rank test).

d. Peripheral blood FACS analysis of CD45.1 recipient mice 6 weeks after transplantion of 100,000 CD19+ cells from lymphoma-bearing *CD19*$^{CRE/+}$*Ezh2*$^{Y641F/+}$ CD45.2 animals.

e. Kaplan-Meier analysis of cancer-free survival of the transplant recipient mice. Donor *CD19*$^{CRE/+}$*Ezh2*$^{Y641F/+}$ CD45.2 Sca1+ hematopoietic progenitors were transduced as indicated and adoptively transferred into sub-lethally irradiated CD45.1 recipient mice. *P* values were calculated using a log rank test.

f. Kaplan-Meier analysis of lymphoma-free survival of *CD19*$^{CRE/+}$*p53*$^{L/L}$ with *Ezh2*$^{+/+}$ vs Ezh2 $^{Y641F/+}$ mice. Median survival for *CD19*$^{CRE/+}$*p53*$^{L/L}$*Ezh2*$^{Y641F/+}$ mice is 159 days ($P < 0.001$, calculated using a log rank test).

g. Enlarged spleens and lymph nodes from CD19^{Cre+} (+/+), *CD19*$^{CRE/+}$*Ezh2*$^{Y641F/+}$ (F/+) and *CD19*$^{CRE/+}$*Ezh2*$^{Y641F/Y641F}$ (F/F) mice.

h. Representative FACS analyses of peripheral blood from (***g***). *C*ircles indicates the abnormal lymphoid population.

i. Western blot analysis and quantification of total H3 and H3K27me3 in control, heterozygous and homozygous *Ezh2*^{Y641F} mice. Error bars show the SEM calculated from three different western blots using separate biological samples. ** $P < 0.01$.

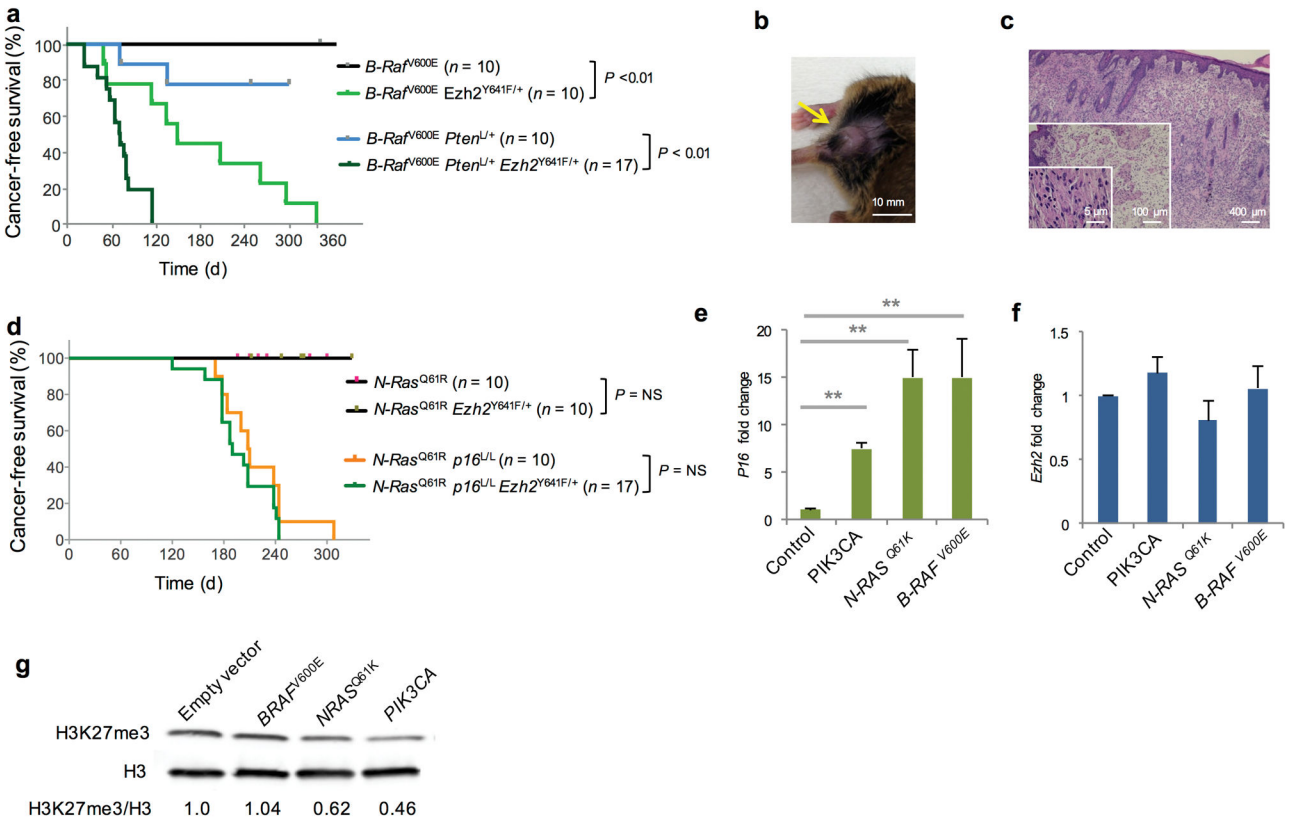

Figure 2. Mutant *Ezh2*^{Y641F} genetically interacts with mutant *B-Raf*^{V600E} but not *N-Ras*^{Q61R} to induce melanoma

a. Kaplan-Meier analysis of melanoma-free survival by indicated *B-Raf* and *Pten* genotypes. *P* values are for the indicated pair-wise comparisons, calculated using a log rank test.

b and **c**. Representative tumor and histological images from tamoxifen-treated *B-Raf*^{V600E}*Ezh2*^{Y641F} mouse. Scale bars as indicated.

d. Kaplan-Meier analysis of melanoma-free survival by indicated *N-Ras* and *p16*^{INK4a} genotypes. *P* values are for the indicated pair-wise comparisons, calculated using a log rank test

e. *p16*^{INK4a} expression in primary human melanocytes transduced with lentiviruses expressing the indicated genes. Averages and SEM from three independent experiments. ** $P < 0.01$

f. *EZH2* expression in primary human melanocytes transduced with lentiviruses expressing the indicated genes. Averages and SEM from three independent experiments.

g. Western blot analysis and quantification of total H3 and H3K27me3 levels in primary human melanocytes transduced with lentiviruses expressing the indicated genes. Representative plot from three independent experiments.

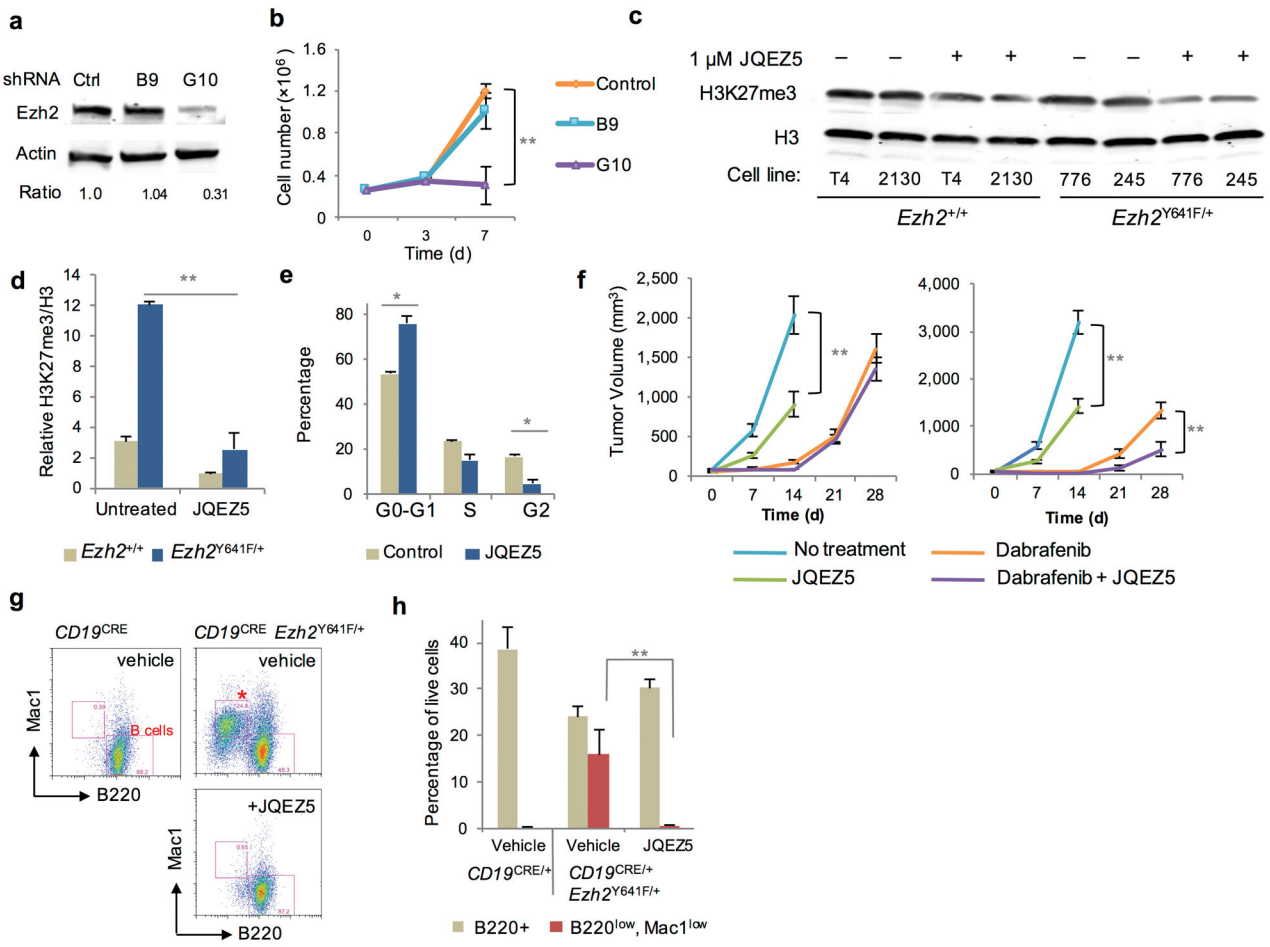

Figure 3. Ezh2 inhibitors demonstrate anti-neoplastic activity in Ezh2^{Y641F}-mutant cancers

a. Western blot demonstrating Ezh2 knock-down in a mouse *Ezh2*$^{Y641F/+}$ melanoma cell line. Control represents scramble shRNA, while significant knock-down was observed with clone G10.

b. Growth curve after *Ezh2* knock-down in a representative mouse *Ezh2*$^{Y641F/+}$ melanoma cell line carried out in triplicate. (Control vs G10, ** P <0.01)

c. Total H3 and H3K27me3 western blots of melanoma cell lines of the indicated *Ezh2* genotype grown in the presence or absence of 1μM JQEZ5.

d. Quantification of the Western analysis in (***c***). Averages and SEM of three independent experiments. ** P <0.01

e. Cell cycle analysis of three *Ezh2* mutant melanoma cell lines cultured for 72 hours in the presence or absence of 1μM Ezh2 inhibitor JQEZ5. * P < 0.05

f. Melanoma tumor volume progression in mice transplanted with *Ezh2*$^{+/+}$ (left) vs *Ezh2*$^{Y641F/+}$ (right) tumor lines. Mice were treated with Dabrafenib, JQEZ5 or a combination of the two once tumors reached 10 mm^3 in size. (n = 8 tumors per group, ** P < 0.01)

g. Representative flow analysis of the spleens of *CD19*$^{CRE/+}$ or *CD19*$^{CRE/+}$*Ezh2*$^{Y641F/+}$ mice. Mice were treated with either vehicle or JQEZ5 for 1 week after they developed

symptoms of lymphoma. Cells were gated on CD19+ cells. Red star indicates the malignant $B220^{low}Mac1^{low}$ population.

h. Quantification of FACS analysis in (***g***). Error bars show the SEM ($n = 5$ mice per group, ** $P < 0.01$).

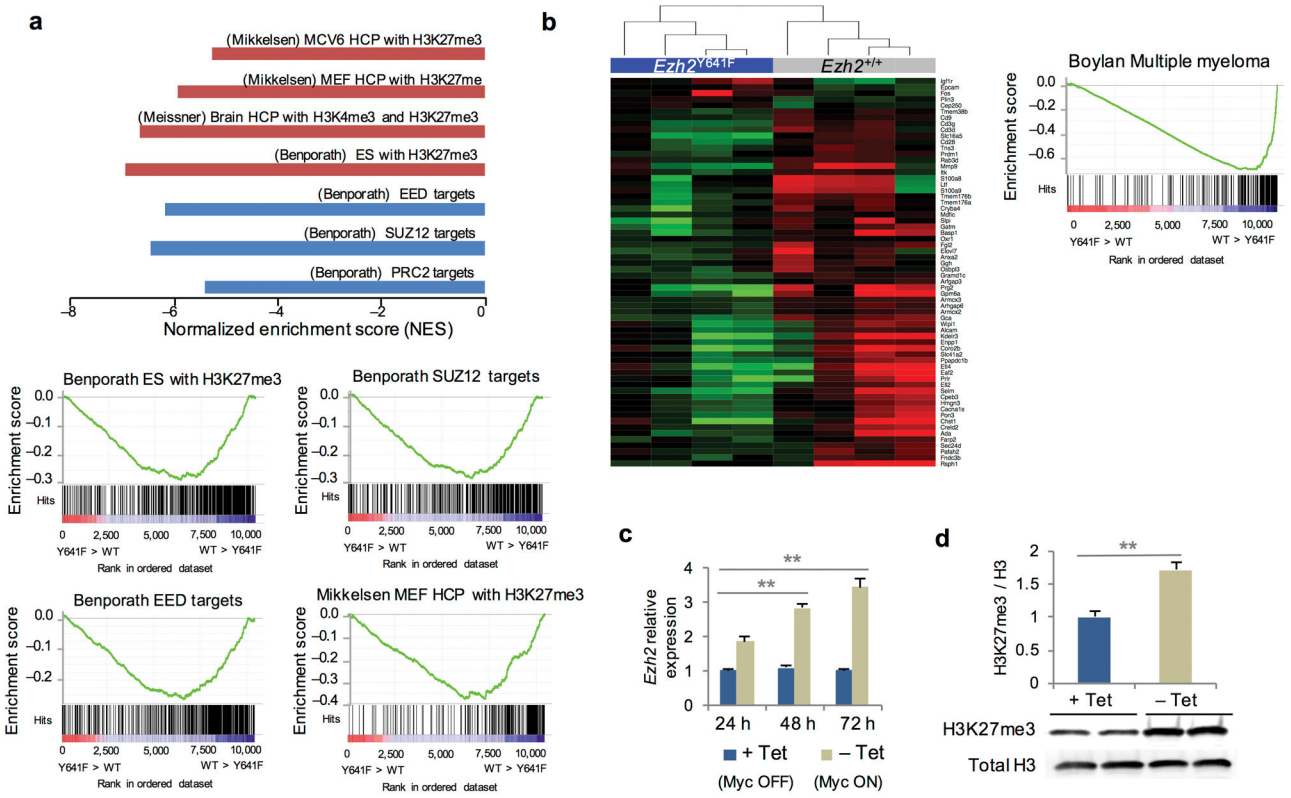

Figure 4. Gene expression in *Ezh2*^{Y641F} reflects enrichment for PRC2 targets, H3K27me3-suppressed genes and a C-MYC signature

a. Gene set enrichment analysis (GSEA) in melanoma cell lines expressing *Ezh2*$^{+/+}$ or *Ezh2*$^{Y641F/+}$. Select significantly enriched gene set plots at $P < 0.01$ and false discovery rate (FDR) < 0.01 are shown with their respective normalized enrichment score (NES).

b. GSEA and heat map comparing expression of genes downregulated in BCL2L1/MYC-driven myeloma [21] to RNA-seq results of *Ezh2*^{Y641F} mutant versus wild-type splenic B-cells. Transcripts repressed by C-MYC in myeloma are also repressed by Ezh2 activation in primary B-cells.

c. EZH2 expression in P493-6 lymphoma cells before and after activation of MYC. Average of three independent experiments.

d. Western blot analysis and quantification of total H3 and H3K27me3 performed on P493-6 cells before and 72h after activation of C-MYC. Error bars reflect the SEM calculated from three different western blots using separate biological samples. ** $P < 0.01$.

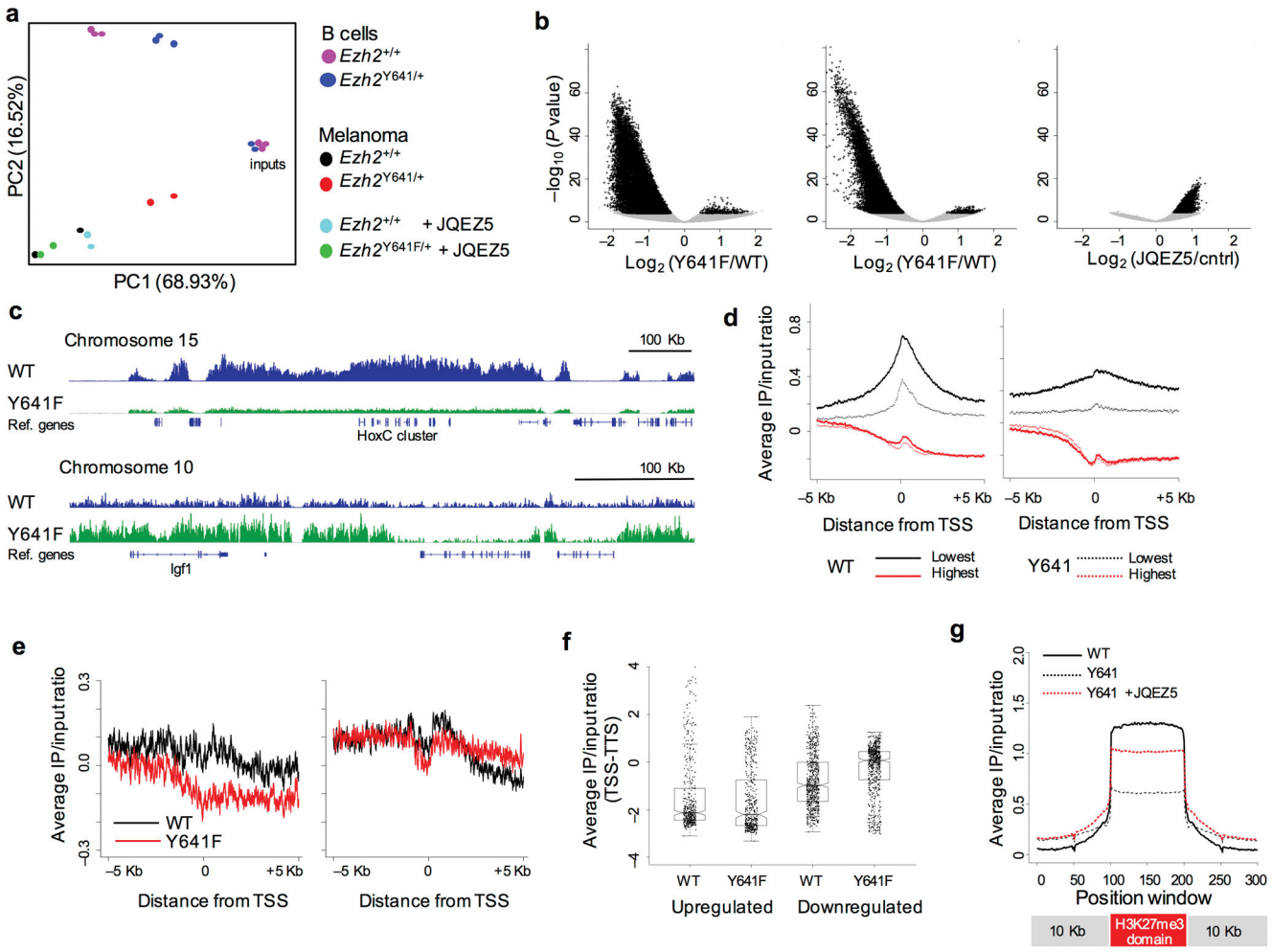

Figure 5. *Ezh2*^{Y641F} changes the genomic distribution and dynamics of H3K27me3

a. Principal component analysis of B-cell and melanoma ChIP-seq data.

b. Volcano plot of H3K27me3 ChIP-seq data displaying the $\log_2$ ratio of *Ezh2*$^{Y641F/+}$ over *Ezh2*$^{+/+}$ signals for each peak (*x*-axis, $\log_2$ values) vs the significance of the differences (*y*-axis, $-\log_{10}$ *P* values). Left – B-cells, Center – melanoma cells, Right –melanoma cells + JQEZ5. The volcano plot on the right displays the $\log_2$ ratio of JQEZ5-treated over vehicle-treated melanoma cells.

c. Representative loci showing decreased H3K27me3 at the *HoxC* locus in B-cells (upregulated), and the Igf1 locus in melanoma cell lines (downregulated).

d. Analysis of H3K27me3 signal at 5 kb upstream and downstream of transcriptional start sites of the bottom 25% (black) and top 25% (red) of genes based on expression in B-cells (left) and melanoma cells (right).

e. Analysis of H3K27me3 signal at 5 kb upstream and downstream of transcriptional start sites of the significantly upregulated (left) and downregulated (right) genes in melanoma samples in the presence of *Ezh2*^{Y641F}.

f. Summary of H3K27me3 signal within gene bodies (TSS–TTS) of upregulated and downregulated genes in the presence of Ezh2$^{+/+}$ vs Ezh2^{Y641F} in melanoma cells.

g. Meta-analysis of the amplitude and distribution of H3K27me3 signal over broad H3K27me3 domains identified in $Ezh2^{+/+}$ melanoma cells. One-hundred variable-width windows cover the peak regions, and one-hundred 100-bp windows cover the 10 kb flanking these regions. H3K27me3 signal is summarized for *Ezh2*$^{+/+}$, *Ezh2*$^{Y641F/+}$ and *Ezh2*$^{Y641F/+}$ + JQEZ5 in melanoma cells.